ORIGINAL ARTICLE

Levelling co-located GNSS and tide gauge stations using GNSS reflectometry

Alvaro Santamaría-Gómez · Christopher Watson · Médéric Gravelle · Matt King · Guy Wöppelmann

Abstract The GNSS reflectometry technique provides geometric information on the environment surrounding the GNSS antenna including the vertical distance to a reflecting surface. We use sea-surface reflections of GPS signals, recorded as oscillations in signal-to-noise ratio (SNR), to estimate the GNSS to tide gauge (TG) levelling tie, and thus the ellipsoidal heights of the TG. We develop approaches to isolate SNR data dominated by sea-surface reflections and to remove SNR frequency changes caused by the dynamic sea surface. Comparison with in situ levelling at eight sites reveals mean differences at the centimetre level for satellites above 12° elevation, with four sites showing differences of 3 cm or smaller. These differences include errors in the in situ levelling, in the antenna calibration model and in the TG measurements, and so represent an upper bound on our technique's error. Data sampling (1 or 30 s) does not significantly affect the results. We detect systematic errors at the decimetre level related to satellite elevations below 12° and to sea-surface height and also differences between results from the L1 and L2 GPS signals larger than 15 cm at two sites. These systematic errors remain unexplained; differences between GPS signals are attributed to receiver-dependent differences in the SNR measurements, while the elevation-dependent error is attributed to unmodelled phase effects such as those caused by tropospheric refraction and sea-surface roughness. Using our approach, we identify a levelling offset of 1.5 cm

A. Santamaría-Gómez (✉) · M. Gravelle · G. Wöppelmann
LIENSs, University of La Rochelle - CNRS, La Rochelle, France
e-mail: alvaro.santamaria@univ-lr.fr

A. Santamaría-Gómez · C. Watson · M. King
School of Land and Food, University of Tasmania, Hobart, Australia

related to a TG sensor change, illustrating our technique's value for TG reference monitoring.

1 Introduction

Since the nineteenth century, coastal observations of mean sea level from tide gauges (TG) have been commonly used as a reference level to establish many national height reference systems. Knowledge of the ellipsoidal height and the geopotential of the TG's reference or zero allows one to determine the mean dynamic topography (MDT) which is an important step towards a world height system (Sánchez 2012; Woodworth et al. 2012). Coastal estimates of MDT are also important to assess errors in national height systems (Amos and Featherstone 2009; Featherstone and Filmer 2012; Penna et al. 2013), to validate geoid models and mean sea-surface models (Andersen and Knudsen 2009; Dayoub et al. 2012; Woodworth et al. 2012) or to complement offshore MDT estimates from satellite altimetry (Madsen et al. 2007; Foreman et al. 2008). Obtaining TG sea-level observations in a common vertical reference frame would also benefit the determination of vertical crustal motion patterns along the coast (Koohzare et al. 2008) as well as sea-level research in coastal ocean circulation, sea-level reconstructions (Church and White 2011; Calafat et al. 2014) and absolute bias determination of satellite altimeters (Watson et al. 2011).

Ellipsoidal heights at TGs are typically obtained from colocated global navigation satellite system (GNSS) tracking stations, mainly global positioning system (GPS) stations, provided the vertical offset or levelling between the reference points of the TG and the GNSS antenna is measured

using classical surveying (levelling) techniques. However, despite being one of the main recommendations within the global sea level observing system (GLOSS) implementation plan (IOC 2012), the number of TGs directly co-located with a GNSS station is very limited. From the 289 TGs of the GLOSS core network (GCN), only 135 (47 %) are within 2 km of a GNSS station from which data are publicly available to the scientific community.[1] The number of co-located GCN TGs with levelling information is further reduced to 65 (22 %). The lack of levelling information is also noticeable in the scientific-quality revised local reference dataset of the permanent service for mean sea level (PSMSL; Holgate et al. 2013) where only 14 % of the active TGs (i.e., supplying data after 2012) are connected with co-located GPS stations. These figures bear witness to the difficulty face by relevant agencies in the use of classical surveying techniques to tie both instruments together. Highly precise geodetic levelling between TGs and GNSS stations requires specialised staff and equipment and in many cases is a complicated task due to the specific location of the GNSS antenna on top of buildings or coastal structures; it can be also very expensive in some TG locations (e.g., small or remote islands) or if the separation distance to the GNSS station is large. Finally, classical levelling assumes that the location of the reference points of both the GNSS and TG instruments are known.

In this paper we explore an innovative approach built on the ground-based GNSS reflectometry (GNSS-R) technique (e.g., Jin et al. 2014) to continuously and remotely determine the vertical offset between the reference points of co-located TG and GNSS stations. Within this technique, the quality and strength of the observed GNSS carrier signals, recorded as signal-to-noise ratio (SNR) measurements, is analysed to extract geometric information pertaining to the nearby reflecting surfaces, in particular their location with respect to the GNSS antenna (e.g., Bilich and Larson 2007). Numerous applications of this technique have emerged in the past decade including inference of snow depth, vegetation growth and soil water content (e.g., Larson et al. 2008, 2009, 2010; Jacobson 2010; Small et al. 2010; Nievinski and Larson 2014b, c). While these studies were based on SNR measured with standard geodetic equipment, Cardellach et al. (2011) provide a list of GNSS-R applications using different approaches and specialized equipment.

Analysis of SNR data has been used to determine the time-varying vertical distance between GNSS antennas and the surrounding dynamic sea surface, effectively transforming coastal GNSS stations into alternative TGs (Anderson 2000; Benton and Mitchell 2011; Larson et al. 2013a, b; Löfgren et al. 2014). A different GNSS-R approach, based on phase analysis rather than SNR and using additional specialized

equipment, was also successfully used to create a GNSS tide gauge (Löfgren et al. 2011a, b; Löfgren and Haas 2014). In some of these earlier studies the SNR-derived sea-surface height (SSH) variations were validated with co-located TG observations, assuming both are sensing the same variations of the sea level, yielding typical standard deviation of differences at the decimetre level (e.g., Löfgren et al. 2014). However, these studies have only considered the relative motion of the sea level and no attention has yet been paid to the absolute SSH values obtained from the GNSS-R technique.

Here, we combine the SSH estimate obtained from SNR measurements (made by commercial geodetic receivers) between the GNSS antenna and the sea surface with the corresponding SSH observed by the co-located TG (see Fig. 1); the result provides the vertical height difference between the reference points of a GNSS and a TG, i.e., the levelling connection, which is missing in many international sea-level programs. By extension, this approach allows the determination of the ellipsoidal height of the mean sea surface observed at the TG. To avoid confusion with the broad range of designations and uses of GNSS reflectometry, from here on we term this new use as "GNSS reflectometry tie" (GNSS-RT). This method provides an automated approach to tie co-located GNSS and TG stations at no additional equipment or field cost, while also facilitating the monitoring for possible instrumental errors. We develop and validate the GNSS-RT approach against existing classical levelling observations using eight case study sites, each presenting different local characteristics such as tidal range, height above the sea surface and equipment types.

2 Methodology

2.1 Background

In this paper we develop an approach based on the geometric model of far-field carrier phase multipath for a single, horizontal, lower-in-height, specular (i.e., considered flat for the GPS carriers), persistent and static reflecting surface (Georgiadou and Kleusberg 1988; Elosegui et al. 1995; Bilich and Larson 2007; Bilich et al. 2007; Benton and Mitchell 2011; Cardellach et al. 2011; Nievinski and Larson 2014b). Following this model, the interferometric phase delay of the reflected signal with respect to the direct signal is given by

$$\psi = \frac{2\pi}{\lambda} 2h \sin e \qquad (1)$$

In this expression ψ is the phase delay, λ is the signal wavelength, e is the satellite elevation and h is the height of the GNSS antenna above the reflecting surface (in the same units as λ). From Eq. 1, and assuming a static reflecting surface (an assumption we address below), the phase delay changes in

---

[1] GNSS data assembly centre for GLOSS (SONEL, http://www.sonel.org), accessed 30 April 2014.
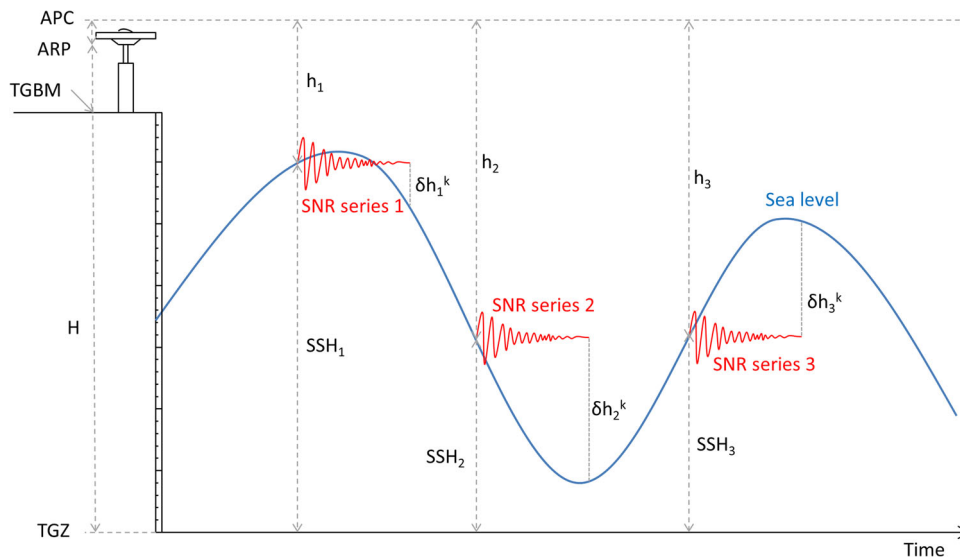
Fig. 1 Simplified schematic diagram of the GNSS-RT levelling. For each SNR series (i), represented by the *red lines*, the levelling (H) is the sum of the sea-surface height (SSH_i), observed from the tide gauge zero (TGZ), and the vertical distance from the antenna phase centre (APC) to the variable sea surface (h_i) represented by the *blue line*. The location of the TGZ is defined by the TG manager and is related to the tide gauge benchmark (TGBM) through the sensor calibration. Similarly, the APC is related to the physically accessible antenna reference point (ARP) through the antenna calibration. The SSH changes with time (represented in the *horizontal axis*) mainly due to tides, being δh_i^k the cumulative SSH change for each SNR measurement k

time as the satellite elevation changes. When the phase delay is a multiple of the signal wavelength, the reflected signal is in phase with the direct signal and the receiver response to the composite signal results in an increased SNR. Conversely, when the phase delay is a multiple of half of the signal wavelength, the reflected signal is out of phase with the direct signal and the resulting SNR of the composite signal being tracked is reduced. Therefore, as the satellite elevation changes with time, the interference pattern between the direct and reflected signals creates a periodic variation in the recorded SNR. The amplitude of the SNR variation is modulated by the antenna gain. At low elevation and assuming similar polarization, the amplitude of the SNR oscillation is higher since the antenna gain is similar for both the direct and the reflected signals for most natural surfaces. As the elevation angle increases, the amplitude of the SNR oscillation is steadily attenuated because the antenna gain for the direct signal progressively dominates within the composite signal.

The frequency of the SNR oscillation depends on the vertical distance to the reflecting surface and the satellite elevation. If one considers the SNR variations against $\sin(e)$ instead of time, then the resulting frequency (ν) of the SNR oscillation is linearly proportional to the height above the reflecting surface (h) (Axelrad et al. 2005; Benton and Mitchell 2011; Larson et al. 2013a):

$$\nu = \frac{2}{\lambda} h \tag{2}$$

Equation 2 allows one to estimate the GNSS antenna height above the reflecting surface by determining the frequency of the SNR oscillation against $\sin(e)$ for each observed satellite arc.

Higher antenna heights above the reflecting surface induce higher frequency oscillations in the SNR series. Following the Nyquist sampling theorem, the highest frequency that could be determined within the SNR series is limited to half the GNSS data sampling frequency. Therefore, the sampling interval of the recorded GNSS data provides the upper limit of the observable GNSS antenna height above the reflecting surface. From Eq. 2, the maximum height of the GNSS antenna above the reflecting surface (h_{max}) is given by

$$h_{max} = \frac{\lambda}{4s}, \tag{3}$$

where s is the unitless SNR sampling with $\sin(e)$, and λ and h_{max} are in the same units. However, Eq. 3 is not an easy-to-use upper height limit because the SNR sampling with $\sin(e)$ is not regular and depends on the elevation and the trajectory (maximum elevation) of each observed satellite. For example, for a single satellite, or for several satellites with similar trajectory, the change in $\sin(e)$ becomes smaller as the elevation increases. For a given satellite elevation, the satellite trajectory also determines the change in $\sin(e)$, becoming smaller when the satellite approaches its maximum elevation with respect to the GNSS antenna. The maximum height h_{max} also depends on the GPS wavelength (λ); this dictates a smaller h_{max} for L1 ($\lambda \approx 0.19$ m) than for L2 ($\lambda \approx 0.24$ m). Considering these determining factors, the lowest bound on h_{max} can be approximated using the $\sin(e)$ increment cor-

responding to L1 SNR observations from a low-elevation (e.g., 5°) and fast-ascending satellite (e.g., a satellite whose trajectory does not reach its maximum below 40°). In this case, h_{max} is ~390 m for data recorded at 1 s, large enough for most GNSS stations installed near TGs; however, it is reduced to ~13 m for data recorded at 30 s. Higher satellites or satellites ascending slowly (with lower maximum elevation) provide a larger upper limit for h_{max}.

The wavelength, the height above the reflecting surface and the satellite elevation also determine the average size of the footprint on the reflecting surface. The reflecting footprint, which is approximated by the first Fresnel zone, is larger for larger wavelengths, higher distances to the reflecting surface and lower elevation satellites (Larson and Nievinski 2013). Considering a specular reflection model in Eq. (1), the location of the reflecting footprint can be approximated by a single reflecting point. From here on, we will use the term reflecting point rather than reflecting footprint while bearing in mind that the actual reflecting area is different.

2.2 GNSS-RT levelling

The proposed approach aims at estimating the time-constant relative height between the reference points of co-located GNSS and TG stations using reflected GNSS signals from the sea surface. Figure 1 is a schematic summary of the parameters utilized throughout this section.

The point in the GNSS antenna where the radio signals are detected is the antenna phase centre (APC). Within an antenna calibration model (e.g., Schmid et al. 2007), the location of the APC is defined with respect to the antenna reference point (ARP), which is a physical point located on the antenna, the vector between the averaged APC and the ARP being the modelled antenna phase centre offset (PCO). To avoid reference changes when the GNSS antenna or its monument is replaced, it is a common practice to refer the GNSS observations to an external marker, though this additional vector will be neglected here for the sake of simplicity. The reference point for the TG measurements is called the TG zero (TGZ) and, through calibration, its location is defined with a known vertical separation from a land-based benchmark positioned near the TG (TGBM) (IOC 2006).

As discussed above, classical levelling between a GNSS and TG station is used to measure the vertical distance between the TGBM and the ARP or the GNSS station marker, and then between the APC and the TGZ assuming their location is perfectly calibrated. Conversely, our approach provides the vertical distance between the APC and the TGZ by adding the observed SSH from the TG (SSH_i) to the estimated GNSS antenna height above the reflecting sea surface from the SNR data (h_i), that is,

$$H_i = SSH_i + h_i + \varepsilon_i, \qquad (4)$$

where H_i is the vertical distance between the APC and the TGZ for the SNR series i. ε_i is the height error that includes contributions from both the GNSS-RT and TG SSH observations.

The proposed pre-processing of the SNR data in our approach is initially similar to earlier studies (e.g., Larson et al. 2013b). Namely, the SNR data for each observed GPS signal are treated independently and then split into ascending and descending arcs up to an elevation of 40°. Arcs shorter than 5 min of duration were rejected. SNR data sampling at both 1 and 30 s were used and treated independently. A fourth-degree polynomial is removed from each SNR series to account for the SNR trend dominated by the contribution of the antenna gain pattern to the measured SNR. This polynomial is sufficiently smooth to not absorb low-frequency SNR oscillations produced when the GNSS antenna is close to the sea surface. From here, the proposed processing of the SNR data differs from earlier studies to specifically address the levelling between the GNSS and TG reference points.

When the sea is the reflecting surface of interest a complication arises since it is not a static surface. Since the frequency of the SNR oscillation varies as a function of the distance to the sea surface (see Eq. 2), each SNR series will experience an inverse Doppler-like effect, i.e., the SNR frequency will reduce for an approaching (rising) sea surface and vice versa. This change in the SNR oscillation frequency is not to be confused with the Doppler frequency change experienced by the reflected wave in comparison to the direct signal which would be produced even with a static reflecting surface (Nievinski and Larson 2014a).

Sea level rises or falls within a range of time scales that depend on the tidal range, the dominant tidal characteristics (diurnal, semi-diurnal, etc.) and the external forcing (i.e., changes in wind, air pressure, etc.). Using short SNR series, Larson et al. (2013b) and Löfgren et al. (2014) estimated a linear frequency drift correction for sites with large tidal range. Unlike those studies, we are not focused on measuring SSH variation independent of a TG, and so we can instead overcome this effect by using the a priori known SSH variations from the TG observations themselves. By adequately modifying the independent variable in the series ($\sin(e)$), one can remove the frequency change of the SNR signal and transform it into a monotonic oscillation. A clear advantage of this approach is that with the SNR frequency change removed, one can benefit from integrating more cycles in long SNR series to improve the estimate of the SNR frequency, i.e., breaking of the satellite arcs is not needed.

Given the known SSH change within a SNR series, the correction for the inverse Doppler-like effect results in the independent variable $\sin(e)$ being stretched or contracted according to

$$\sin(e_i^k)' = \sin(e_i^k)\left(1 - \frac{\delta \nu_i^k}{\nu_i}\right)$$

$$\delta \nu_i^k = \int \frac{2}{\lambda} \delta h_i^k, \tag{5}$$

where $\sin(e_i^k)'$ is the value of the independent variable after correction for the inverse Doppler-like effect. Sub-scripts i refer to each SNR series and super-scripts k denote each individual SNR measurement in the series. ν_i is the instantaneous frequency and $\delta \nu_i^k$ is the cumulative frequency change for each SNR measurement from the beginning of the series, estimated from the SSH change with $\sin(e)$ and Eq. 2. The cumulative frequency change is accounted for relative to the chosen instantaneous frequency. We set the instantaneous frequency at the beginning of the SNR series, although there is no difference if a different convention is chosen (e.g., adopting the end or the middle of the SNR series).

After correcting the SNR series for the inverse Doppler-like effect, the estimation of the SNR frequency (ν) is performed in two separate steps. First, we estimate the spectra for all the SNR series and iteratively stack them in 24 h periods (Sect. 2.2.1). For the stacking, all the spectra are reduced to a common height level to remove the difference in the instantaneous frequency among the SNR series produced from variations of the SSH. The stacking of the spectra provides an a priori daily value of the levelling H. Second, using the a priori value for H, we estimate the frequency of the SNR oscillation (h_i) for each SNR series through a non-linear least-squares minimization (Sect. 2.2.2). For the SNR frequency estimation, we apply a Kalman filter to automatically isolate the SNR data containing significant reflections from the sea surface. From this step, Eq. (4) provides an estimate of the levelling (H_i) per selected SNR series. To determine the final estimate of H, we take the weighted mean of the H_i estimates, with the relative weight of each H_i taken from the explained SNR variance after the least-squares fit.

2.2.1 First pass: stacking of the SNR spectra

The objective of the stacking of the SNR spectra is to generate a precise a priori estimate of the levelling (H) without the necessity of using external information pertaining to the station height other than the recorded SNR and the TG observations. This a priori levelling value is used in Sect. 2.2.2 to isolate the SNR oscillations produced by reflections off the sea surface from other reflectors and to subsequently carry out the estimation process for levelling.

The power spectrum of each SNR series was estimated using the Lomb normalized periodogram approach (Press et al. 2001). By stacking the spectra from all the satellite arcs, the peaks of reflectors located at the same height add constructively over the background noise. Hereafter, we refer to the SNR data not corrected for the inverse Doppler-like effect, and their spectra, as 'raw' series and spectra, respectively. Due to the SSH change, the sea-surface reflections will add partially destructively in the stacking of the raw spectra, whereas reflections from the ground beneath the antenna and other static reflectors will add constructively. This effect can be removed by first correcting the SNR series for the inverse Doppler-like effect following Eq. 5 and then by shifting each computed spectrum prior to stacking by a frequency offset corresponding to the known SSH (SSH$_i$ in Fig. 1) at the chosen instantaneous SNR frequency (ν_i in Eq. 5). We refer to these as 'corrected' series and 'reduced' spectra, respectively. The SSH$_i$ corresponding to the epoch of the instantaneous SNR frequency is linearly interpolated from the TG record. When correcting for the inverse Doppler-like effect, the instantaneous SNR frequency (ν_i) is actually the parameter of interest and thus is unknown. This value can be approximated iteratively until the peak of the stacked spectra converges to a predefined level (e.g., 1 mm). The a priori value for the instantaneous SNR frequency can be set by inspecting the stacked raw spectra. Typically, the peak converges in less than five iterations. By iteratively stacking the reduced spectra of the corrected SNR series, all the contributions from static reflectors (e.g., the ground beneath the antenna) add destructively since their reflections are no longer at a constant height. Conversely, the power of reflections from the sea surface is enhanced now since the sea is the only reflector at a constant height among all the satellite arcs overpassing the sea surface. Since the SSH observations are referred to the TGZ, the SNR frequency of the peak from the stacked reduced spectra provides an approximate value of the levelling (H) following Eq. 2.

To illustrate the approach, we examine the stacked spectra for two GNSS sites representing two extremes in tidal range. Marseille (MARS), located on the Mediterranean French coast, has a tidal range of less than 0.5 m, whereas Brest (BRST), located on the Atlantic French coast, has a tidal range up to 7 m (Table 1). Figure 2 presents their stacked SNR spectra. The dotted black lines in Fig. 2 represent the stacking of the raw spectra where the SNR frequency is transformed into height using Eq. 2. For both cases, the stacking of the raw spectra shows increasing power from reflections located very close to the GNSS antenna, such as the ground surface below the antenna, or due to imperfect detrending of the SNR data. Significant power is also found at heights close to that expected for the sea surface. The peak at the sea-surface height is narrower for MARS than for BRST as this station exhibits almost no tide, whereas for BRST the power at the sea-surface height is spread given the (uncorrected) extreme tidal range at this site. The dashed red lines in Fig. 2 represent the result of stacking the reduced spectra from raw series (not corrected for the inverse Doppler-like effect); the peak in the stacked spectra is now shifted to the right corresponding to the addition of the SSH measured by the TG,

Table 1 Location, equipment, daily tidal range and the approximate antenna height above the sea surface for each case study site during 2013

Site	Lat.	Long.	GNSS, receiver	GNSS, antenna and radome	TG, sensor	Tidal range (m)	Reflector height (m)
Brest (BRST)	48.38	−4.50	Trimble, NETR9	Trimble, TRM57971.00, NONE	Radar, Krohne	2.0–6.9	13–20
Burnie (BUR2)	−41.05	145.91	Leica, GRX1200	Leica, LEIAT504, SCIS	Acoustic, Aquatrak	1.8–3.4	4–7
Marseille (MARS)	43.29	5.35	Leica, GR25	Trimble, TRM57971.00, NONE	Radar, Optiflex	0.1–0.4	12–13
Roscoff (ROTG)	48.72	−3.97	Topcon, TPS GB-1000	Topcon, TPSGB-1000, NONE	Radar, Optiflex	2.4–8.4	5–13
Socoa (SCOA)	43.39	−1.68	Leica, GR25	Trimble, TRM55971.00, NONE	Radar, Optiwave	1.4–4.4	9–12
Saint-Malo (SMTG)	48.64	−2.03	Topcon, TPS GB-1000	Topcon, TPSPG_A1+GP, NONE	Radar, Optiwave	3.2–12.0	8–19
Spring Bay (SPBY)	−42.55	147.93	Leica, GRX1200	Leica, LEIAT504GG, SCIS	Acoustic, Aquatrak	0.5–1.3	3–5
Tarifa (TARI)*	36.01	−5.60	Leica, GRX1200	Leica, LEIAR25, NONE	Radar, Miros	0.4–1.6	8–9

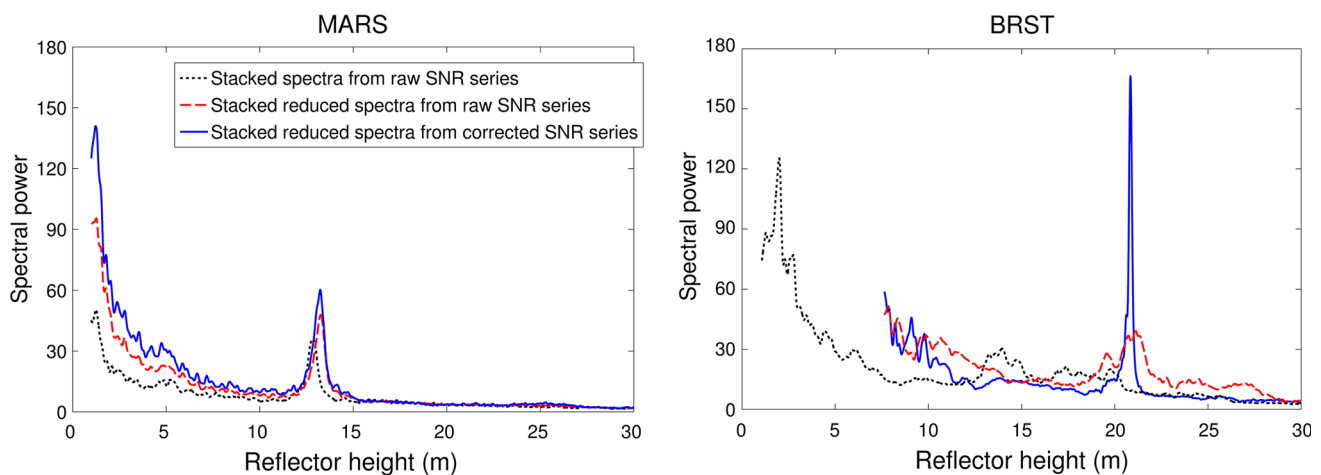Asterisk indicates details for Tarifa corresponding to January–April 2014

Fig. 2 Stacked spectra of observed L1 SNR data at 1 s sampling on 3 January 2013 at MARS (*left*) and BRST (*right*) stations. The *dotted black lines* represent the stacking of the raw SNR spectra derived from multiple satellite arcs. The *dashed red lines* represent the stacking of the reduced spectra from raw SNR series. The *solid blue lines* represent the stacking of the reduced spectra from the inverse Doppler-like corrected SNR series

which is usually always positive. In this case, the power from reflections at the SSH is increased at both stations. The peak is still narrower for MARS than for BRST because the SNR frequency at MARS does not change within the series (due to the tidal range and inverse Doppler-like effect) as much as at BRST. The solid blue lines in Fig. 2 represent the result of stacking the reduced SNR spectra from the corrected SNR series. A well-resolved peak appears now in the BRST spectrum (Fig. 2, blue line) providing a more precise a priori estimate of the levelling (H).

This approach is significantly different from earlier studies that focused on time-variable SSH and where the inverse Doppler-like effect within the SNR series was a nuisance for estimating the SNR frequency corresponding to the SSH (e.g., Larson et al. 2013b; Löfgren et al. 2014). In our application, given the focus on the GNSS to TG tie, the TG observations provide valuable information to obtain precise fre-

quency estimates. An important finding from these examples is that sites with higher tidal range yield a narrower peak in the stacked corrected spectra, i.e., the larger the tidal range, the more decorrelated the static surfaces around the antenna are from sea surface. Consequently, the advantages of this automatic approach may vanish for specific sites where the sea surface mimics the ground surface, i.e., the water surface very close in height to the ground coupled with a negligible tidal range, as in lakes or reservoirs.

2.2.2 Second pass: frequency optimisation

Using the a priori daily value for H from the stacked spectra of Sect. 2.2.1, the next step is to extract the SNR data containing clear reflections produced on the sea surface and estimate the frequency and associated quality of the selected SNR oscillations per observed satellite.
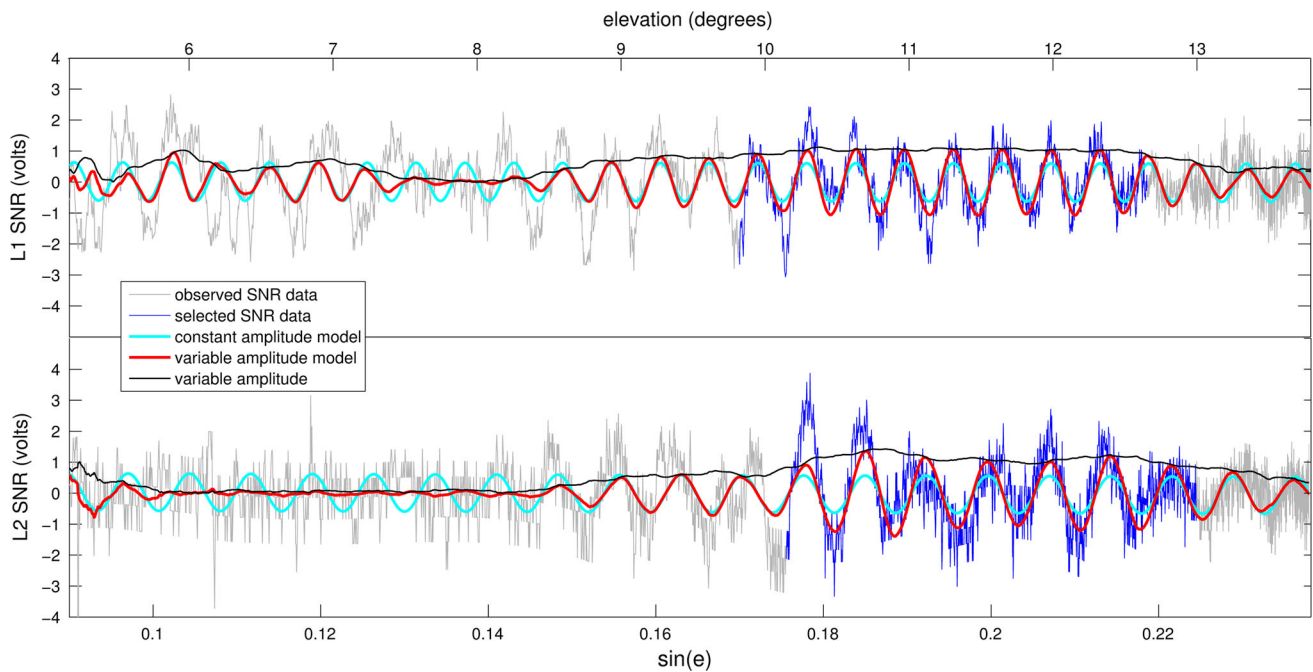
Fig. 3 SNR data for satellite PRN21 observed at station BRST on 13 January 2013 for the L1 (*upper*) and the L2 (*lower*) GPS signals. The *grey lines* represent the detrended and inverse Doppler-like corrected SNR series with respect to the satellite elevation [sin(*e*)]. Note the different behaviour of the low-elevation SNR measurements in L2 compared to L1. The *cyan lines* represent the fitted constant-amplitude sinusoidal model. The *red lines* represent the fitted variable-amplitude sinusoidal model from the Kalman filter, with the *black lines* representing the time-variable sinusoidal amplitude from the same filter. The *blue lines* represent the selected segments of SNR data

To achieve this, we first took each corrected SNR series and fitted a sinusoidal model with constant amplitude through non-linear minimization of the sum of the squared residuals. The a priori SNR frequency, corresponding to the APC height above the sea surface (h_i), was obtained by subtracting the SSH at the beginning of the arc (SSH_i) from the a priori levelling value (H). The minimization of the frequency was bound within ±40 cm from the a priori h_i value, with this threshold chosen empirically based on the daily repeatability of stacked spectra and on the scatter of the frequency estimates per satellite arc. The frequency and phase of the fitted sinusoid with constant amplitude were then fixed and used to estimate a varying amplitude, modelled with a random walk process noise of amplitude 1 V/sin(e)^2 through a Kalman filter. This process noise level is large enough to capture not only the steady change of the amplitude in the SNR oscillation with satellite elevation, but also abrupt SNR amplitude changes. The latter may arise due to the appearance and disappearance of the sea surface reflections caused by irregular obstacles surrounding the station or to tracking issues unrelated to the reflecting environment (e.g., codeless tracking losses). Only the segments of the SNR series having SNR oscillation amplitude higher than the scatter of the residuals from the fit were selected for subsequent analysis. This amplitude threshold is arbitrary and choosing a different value will impact the amount and quality of the data retained in the analysis. In addition, to ensure a correct frequency esti-

mate, we chose to only retain those segments with at least three complete SNR cycles. Since both L1 and L2 GPS signals must provide SNR oscillations from the same reflector, the minimum of three complete SNR cycles applies to both L1 and L2 signals within the same range in elevation, that is, satellite arcs with a minimum of three valid SNR oscillations were not retained if they were present in only one of the GPS signals or in both GPS signals but at different elevation.

Figure 3 shows an example of the selection of SNR segments observed at station BRST. For the observed satellite arc, the constant-amplitude and varying-amplitude sinusoid models (cyan and red lines, respectively) were fitted to the observed SNR data in both L1 and L2 signals (grey lines). The time-varying amplitude of the sinusoid is also shown (black lines). For both L1 and L2 signals, a segment of SNR data (blue lines) was retained between 10° and 13° elevation. While the selected SNR segments are not exactly equal in length, both contain at least three complete SNR cycles at a common elevation.

We assume that the resulting selected segments of SNR series are dominated by reflections from the sea surface. Therefore, the automated GNSS-RT technique avoids the need for screening the SNR data or having a priori knowledge of the environment of the GNSS station to mask the satellite arcs being used in the analysis. As an example, Fig. 4 shows the location of reflecting points for each of the selected segments of SNR data at stations BRST (left) and BUR2 (right)
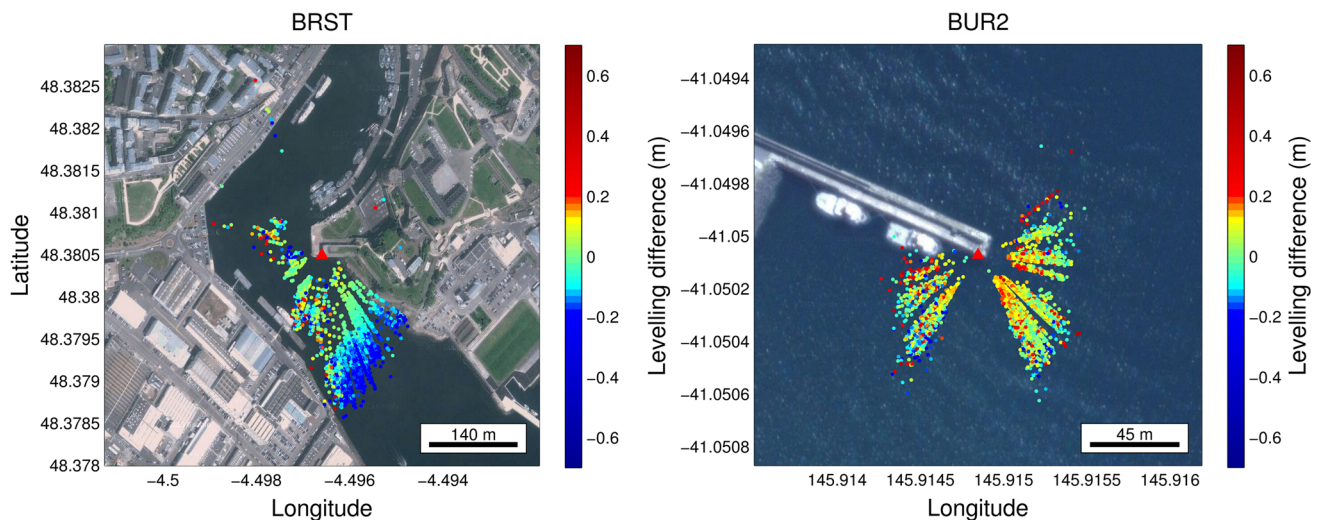
Fig. 4 Location of the reflecting points for each selected SNR series at BRST (*left*) and BUR2 (*right*) stations. The *colour scale* represents the GNSS-RT levelling differences (in metres) with respect the nom- inal levelling value at each site. Note for BUR2, the sector devoid of reflections immediately to the south of the GPS site is commensurate with the southern hole in the constellation geometry at this latitude

for the whole year 2013. Each dot in Fig. 4 represents an estimate of the levelling value H, with the colours show- ing the difference with respect to the nominal value (level- ling results are shown below). Despite the complicated envi- ronment yielding irregular reflections from the sea surface at some stations (e.g., BRST), the reflecting points of the selected segments of SNR series are correctly located on the sea surface, although not all the observed satellite tracks over the sea surface passed the selection criteria.

Once the segments of SNR series were selected, the constant-amplitude sinusoid fitting was repeated to estimate the final instantaneous frequency of the SNR oscillations per satellite arc. These instantaneous SNR frequencies were then transformed into height (h_i) and added to the SSH_i to yield the levelling value H_i per satellite arc (Fig. 1). The nominal value of the antenna phase centre offset (PCO) for each GPS signal was subtracted to provide the GNSS-RT levelling to the antenna reference point. Antenna phase centre variations (PCV) in elevation and azimuth are not considered as they are at the millimetre level; the average PCV for the vertical com- ponent is even smaller and thus neglected. Note that this latter step is applied here to validate the GNSS-RT results against in situ levelling measurements. The GNSS-RT technique pro- vides the levelling connection directly to the average phase centre, thus avoiding errors in the calibrated antenna phase centre values.

3 Case study sites

The approach described in Sect. 2 has been implemented and assessed at eight co-located sites recording both TG and SNR data for the legacy L1 and L2 GPS signals (no L2C) using

commercial equipment. Table 1 provides the location, the equipment (GNSS receiver/antenna and TG), the minimum and maximum sea-level daily tidal range and the approximate antenna height range above the sea surface for each case study site. Aerial views of the surroundings of the case study sites are provided in the supplemental material (Fig. S1). The separation distance between the co-located GNSS and TG for all case study sites is of a few meters, except for Brest (BRST) and Tarifa (TARI) where the separation distances are less than 300 and 100 m, respectively.

We considered all SNR data recorded from 5° to 40° ele- vation from all directions. The elevation cut-off was set to 40° as no significant SNR oscillations were found at higher elevation angles. Since the SSH_i values are linearly interpo- lated in the TG record (see Sect. 2.2.1), days with less than 90 % of available TG data were rejected.

Classical levelling measurements between the GNSS marker and the TG benchmark were retrieved from the SONEL database[2] for each site, from where the nominal levelling between the ARP and the TGZ were computed and used as ground truth. The antenna PCO values in both GPS carriers were taken from the International GNSS Ser- vice (IGS) absolute antenna calibration compilation as per GPS week 1745 (Schmid et al. 2007).

These eight case study sites were selected based on the public availability of classical levelling measurements and high-frequency GPS and TG observations. We used GPS data sampled at high (1 s) and low (30 s) rates for the whole year 2013 for all sites except TARI where GPS data at 1 s were only available between January and April 2014 (30 s data were also limited to this period at TARI). TG

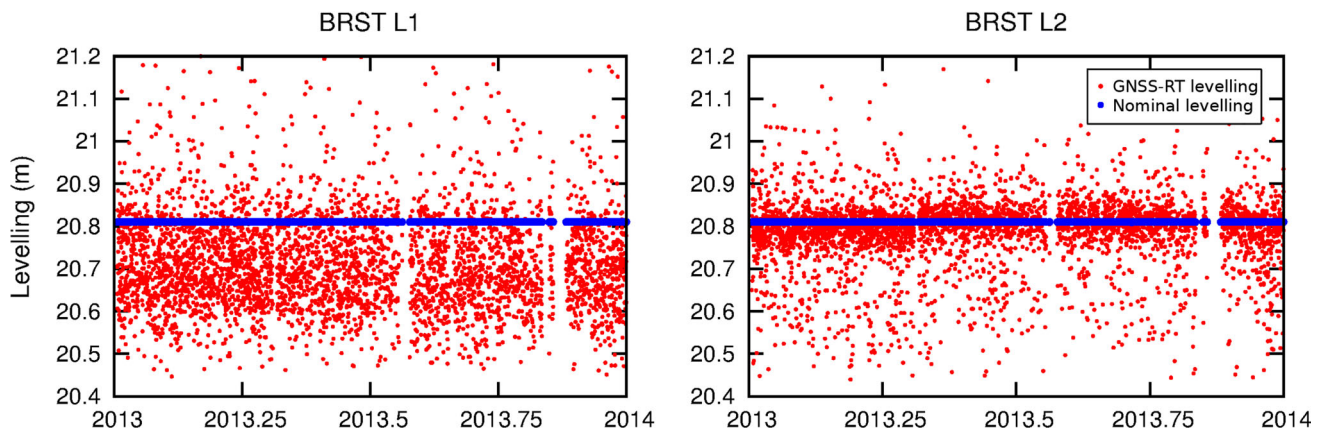
[2] http://www.sonel.org/-Stability-of-the-datums-.html.

Fig. 5 GNSS-RT levelling time series at station BRST for L1 (*left*) and L2 (*right*) GPS signals. The *red dots* represent the GNSS-RT levelling estimate for each selected SNR series. The *blue line* represents the nominal levelling value obtained by classical levelling

data sampling varied between 6 and 10 min at each site and was used for the same period. We note that some sites have particular conditions, making them interesting for the assessment of the GNSS-RT levelling approach. For instance, in Brest (BRST), the mean height of the GNSS antenna above the sea surface exceeds 16 m while the sea surface is tightly enclosed by the port structure (see Fig. 4); in Marseille (MARS), there is almost no tidal range and the antenna location on the TG building roof limits the sea-surface reflections to low-elevation satellites;[3] in Saint-Malo (SMTG) the reflections from the sea surface are blocked by many obstructions (fixed and floating) while the tidal range is one of the world's highest (more than 12 m); in Socoa (SCOA) and Tarifa (TARI) a wide range of sea-surface reflections are available without obstructions; finally, in Burnie (BUR2) and Spring Bay (SPBY), the antenna height above the sea surface is the lowest among all the co-located GNSS sites in the SONEL database, and the reflecting sea surface is more representative of open-sea conditions where the assumption of a flat reflecting surface is more tenuous.

4 Results

We applied the proposed approach to derive time series of GNSS-RT levelling for each case study site of Sect. 3. The supplemental material contains the time series (Fig. S2) and the location of the reflecting points of each levelling estimate (Fig. S1) for each case study site.

As an example of the GNSS-RT levelling results, Fig. 5 shows the levelling time series for the year 2013 obtained at station BRST for the GPS L1 and L2 signals. These results

_____
[3] See MARS pictures at http://www.sonel.org/spip.php?page=gps&id Station=735.

represent the separation distance between the TGZ and the ARP so that results for both L1 and L2 signals can be compared. The in situ levelling value is represented by a blue line; here we assume this nominal value is error-free and thus represents a truth for our approach.

The GNSS-RT levelling time series are scattered around a mean value (Fig. 5 and Fig. S1). The detection and removal of outliers can be easily performed based on the dispersion of the estimates per station and GPS signal. However, the time series exhibit significant differences in the mean value and scatter of the GNSS-RT levelling results between the L1 and L2 signals (Fig. 5 and Fig. S1). Table 2 summarizes the results for all the case study sites showing the weighted mean difference with respect to the nominal levelling value and the weighted standard deviation. Considering all sites, the L1 absolute differences range from 0.9 to 18.1 cm, with a median value of 10.4 cm; and the L2 absolute differences range from 0.2 to 28.6 cm, with a median value of 4 cm. The absolute L2 maximum and median reduce to 8.7 and 2.3 cm, respectively, when the SMTG station is removed (discussed in Sect. 5). The square root of the median variance of the levelling estimates per satellite arc is 12 cm for all sites in both L1 and L2. Nevertheless, excluding SMTG and ROTG stations (see Sect. 5) the scatter of the levelling results varies considerably across the case study sites from 7 to 15 cm with a clear negative correlation with the tidal range, in agreement with the inverse Doppler-like correction (see Sect. 2.2.1 and Fig. 2).

The weighted mean difference between the GNSS-RT levelling and the nominal levelling for most of the sites in Table 2 is significantly different from zero. From the results in Table 2 one may conclude that the GNSS-RT levelling results have in general a negative bias, being smaller for L2 than for L1; the L1 and L2 results for TARI and L1 for BUR2 and SPBY are the only exceptions, exhibiting positive biases.

Table 2 GNSS-RT levelling results for data sampling at 1 s

Station	In situ levelling (m)	L1		L2		#Arcs (%)
		Mean (cm)	Std (cm)	Mean (cm)	Std (cm)	
BRST	20.810	−10.7 (−3.3)	10.6 (11.4)	−2.0 (−0.3)	7.6 (5.1)	4,167 (12)
BUR2	7.298	5.9 (10.7)	11.2 (5.4)	−8.7 (−4.8)	10.0 (5.8)	5,547 (15)
MARS	13.283	−18.1 (−5.7)	14.1 (18.7)	−8.4 (4.9)	15.6 (20.2)	8,520 (29)
ROTG	13.953	−13.8 (−1.8)	16.3 (11.6)	0.2 (2.0)	16.5 (11.6)	4,072 (11)
SCOA	12.858	−10.2 (−1.4)	10.2 (3.4)	0.6 (1.5)	7.1 (3.5)	8,659 (30)
SMTG	20.630	−9.7 (−5.0)	14.0 (12.0)	−28.6 (−23.2)	19.7 (21.6)	2,185 (6)
SPBY	5.720	11.4 (12.7)	11.4 (8.5)	−5.6 (−6.7)	12.7 (11.1)	7,868 (22)
TARI	8.943	0.9 (−2.4)	12.7 (7.9)	2.3 (1.6)	13.3 (5.4)	2,083 (23)

Mean difference values (L1 and L2) are GNSS-RT estimate minus nominal levelling value (in situ levelling plus PCO values). Std is the standard deviation of the GNSS-RT estimates. Mean and standard deviations in parenthesis are for satellite arcs with mean elevation above 12°. #Arcs are the total number of arcs retained with the percentage of retained/observed satellite arcs in parenthesis
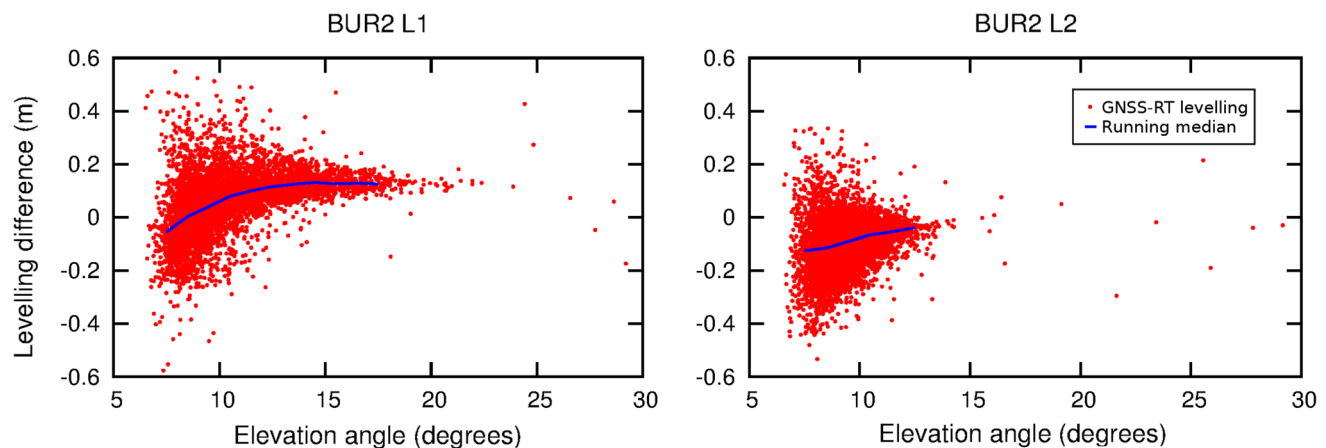

Fig. 6 GNSS-RT levelling differences against the mean satellite elevation per arc at BUR2 station for L1 (*left*) and L2 (*right*). The *red dots* represent the GNSS-RT levelling difference with respect to the nominal value for each selected SNR series. The *blue lines* represent the non-overlapping running median with 1° elevation windows

Although the GNSS-RT levelling time series look stationary (Fig. 5), when plotting the levelling differences with respect to the mean satellite elevation, a clear non-stationary behaviour is revealed, hampering the use of the statistical measures that assume stationarity to assess the levelling results. For instance, Fig. 6 shows the L1 and L2 GNSS-RT levelling differences with respect to the mean satellite elevation of each estimate for station BUR2. To examine the elevation-dependence more closely, we computed a non-overlapping running median of levelling values with 1° elevation windows for each carrier at each site (blue lines in Fig. 6). Elevation windows with less than 30 estimates were not considered. Figure 6 reveals that the central tendency of the BUR2 result is not stationary with elevation angle. The levelling results with respect to the satellite elevation for all the case study sites are provided in the supplemental material (Fig. S3) and they are summarised in the upper half of Fig. 7. For the L1 GNSS-RT levelling results (left

panels in Fig. 7), all sites exhibit a change in the median towards higher values as the mean elevation of each satellite arc increases. The elevation-dependency behaviour of the L1 results is clearly visible when mapping the GNSS-RT levelling differences as a function of the horizontal distance to the GNSS antenna (Fig. 4 and Fig. S2), where the horizontal distance is a function of the GNSS antenna height (at the epoch chosen for the instantaneous SNR frequency) and the mean satellite elevation for each selected SNR series. For all stations except BUR2 and SPBY, the difference with respect to the nominal value reduces as the mean satellite elevation of each arc increases. For BUR2 and SPBY the pattern is the same; however, the median difference converges to a positive bias close to 10 cm. In L2 (right panels in Fig. 7), the elevation dependency is also present but less clear than in L1, with some stations not converging (e.g., ROTG, SPBY) or showing less elevation dependency (e.g., SCOA, TARI).
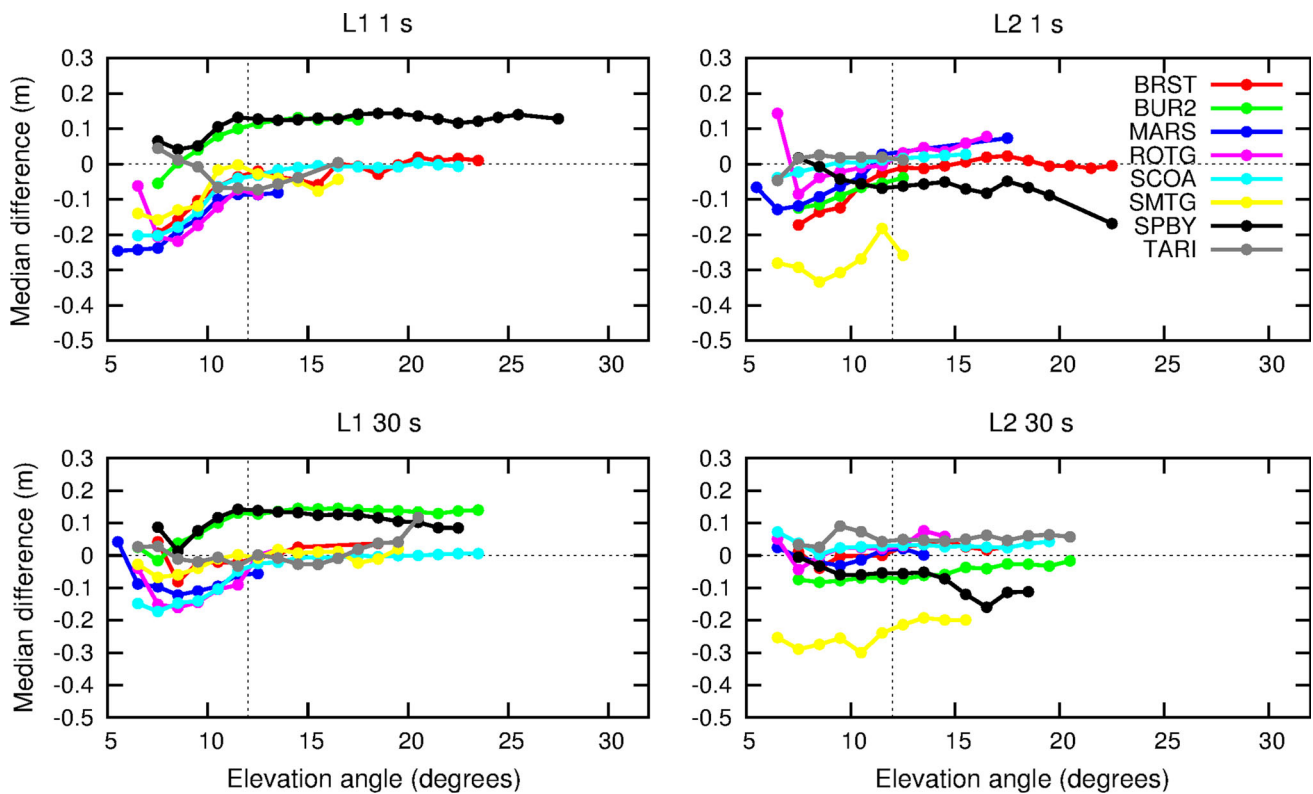
Fig. 7 Non-overlapping running median of the GNSS-RT levelling differences with respect to satellite elevation for each case study site for L1 (*left*) and L2 (*right*). Results for 1 and 30 s data sampling are shown in the *upper* and *lower panels*, respectively. The *vertical dashed line* represents 12° elevation

As an example of the impact of the elevation-dependent behaviour on the GNSS-RT levelling results, the weighted mean difference and standard deviation were repeated but considering only levelling estimates from selected SNR series with a mean elevation above 12°. This threshold is chosen empirically for this exercise based exclusively on the results of Fig. 7 without providing, at this stage, a physical explanation. The outcome for MARS and SMTG sites is less meaningful since very few levelling estimates above 12° were obtained for these two stations (see Fig. S3). The resulting absolute differences in L1 now range from 1.4 to 12.7 cm, with a median value of 4.2 cm. The absolute L1 maximum and median differences reduce to 5.7 and 1.4 cm, respectively, when BUR2 and SPBY stations are not considered (see discussion below). For L2 the absolute mean differences now range from 0.3 to 6.7 cm, with a median value of 2.0 cm (SMTG excluded). The square root of median variance of the levelling estimates reduces to 8.0 cm for both L1 and L2.

In addition to using high-frequency (1 Hz) GPS data, the GNSS-RT levelling technique was assessed using GPS data recorded at the lower and more common rate of 30 s. In Sect. 2.1 we approximated that GNSS data sampled at 30 s could still be used for antenna heights less than 13 m

above the sea surface and that an even higher limit could be reached for some satellite arcs at high elevation or with slow increments of elevation (i.e., close to their maximum elevation).

GNSS-RT levelling results based on 30 s sampling were obtained for all the case study sites; however, in BRST almost none of the satellite arcs were retained when the SSH was lower than 5 m, which represents the GNSS antenna being more than 16 m above the sea surface. This threshold is slightly higher than that predicted in Sect. 2.1 partly because sea-surface reflections in BRST were obtained from satellite arcs at high elevation. For all sites, the GNSS-RT levelling using the 30 s data provide similar results to those obtained with 1 s sampling, with a summary provided in the lower panels of Fig 7. In L1, the absolute difference of the weighted mean with respect to the nominal levelling value per station ranges from 0.1 to 14.0 cm, with a median value of 8.0 cm; and from 0.4 to 5.8 cm, with a median value of 4.2 cm for L2 (SMTG removed). The elevation-dependency of the GNSS-RT levelling in L1 is replicated using the 30 s data, as well as the biased results for BUR2 and SPBY (Fig. 7). The scatter of the levelling estimates is higher when using the 30 s data, with a square root of median variance of 14.4 cm compared to 12.0 cm.

These results indicate that for GNSS antennas close to the sea surface (i.e., less than ~15 m), SNR data sampled at 30 s could be used for GNSS-RT levelling whenever the 1 s data are not routinely available, but higher rate sampling will provide more precise estimates. Using the 30 s data does, however, allow the application of this approach to many more sites that do not track or archive GNSS observations at high sampling rates.

5 Discussion

The mean levelling differences shown in Table 2 are in the centimetre-to-decimetre range and vary among the sites studied, the elevation of the satellites and the GPS signal adopted. These levelling differences include errors related to the estimated antenna height above the sea surface from the GNSS-RT technique, but they may also include errors in the TG data or in the nominal levelling values.

Errors in GNSS-RT derived levelling estimates are produced by unmodelling of the interferometric phase measured by the GNSS receiver. The analysed SNR oscillation may be sensitive to additional unaccounted phase effects besides the geometric contribution being modelled by Eq. 1. Such non-geometrical phase effects include atmospheric refractivity, surface roughness and antenna/surface response (Nievinski and Larson 2014b).

Errors in the nominal levelling values include errors in the in situ levelling and in the antenna vertical phase centre offset (PCO) values. Note that the GNSS-RT technique directly ties the averaged antenna phase centre (APC) of each GPS carrier with the TG reference (TGZ), i.e., no antenna model is needed. Conversely, classical levelling provides the vertical distance between the antenna reference point (ARP) and the TG benchmark (TGBM), i.e., a model for the vertical PCO values is needed when comparing with the GNSS-RT results. We examine these sources of error separately.

5.1 Errors in the estimated height from GNSS-RT

Errors in the estimated height above the reflecting sea surface may result from unmodelled phase effects in the geometric multipath model of Eq. 1. Given that the interferometric phase is driven by the satellite elevation, the elevation-dependent signature found in the GNSS-RT levelling results (Fig. 7) points towards imperfections of the geometric model.

Phase effects from sea-surface roughness and swell are not taken into account in the geometrical model and they exhibit an elevation-dependent signature, being larger for low-elevation observations (Nievinski and Larson 2014a). Sea-surface roughness breaches the flatness or specularity requirement of the modelled SNR oscillation, whereas swell is a series of waves with longer wavelength breaching the horizontality requirement.

When the scale of the vertical sea-surface roughness is significant compared to the GNSS signal wavelength, the GNSS signals are not reflected specularly within the illuminated footprint, but reflected diffusely at random areas outside the assumed illuminated footprint. These secondary reflections are not accounted in for the geometric model and may contaminate the observed convoluted phase.

The presence of swell shadows low-elevation signals and causes the reflecting area to not being illuminated homogeneously (Bourlier et al. 2006; Nievinski and Larson 2014a). The preferred illuminated surface crests over the surface troughs would produce an apparent reflector closer, in agreement with our results. Quantifying the slopes of the swell at wavelengths larger than the signal carrier would allow one to take this effect into account, or at least to determine the lowest elevation angle for which this effect can be neglected.

Different effective scales of sea-surface roughness and swell may be responsible for the imperfect level of agreement between the recorded SNR data and that expected from a geometric model that assumes reflections from a flat and horizontal surface. The median value of the explained variance from the sinusoid fit to the selected SNR data is 53, 61, 34 and 43 %, respectively, at BRST, ROTG, SCOA and TARI sites. These four sites all have a protected environment where the sea surface surrounding the GNSS antenna is enclosed within a port. On the other hand, for BUR2, MARS and SPBY, where the SNR reflections are produced from exposed sea surface, the median value of the explained variance decays to 26, 28 and 33 %, respectively. This outcome is consistent with increased noise content expected in the SNR measurements from exposed-sea conditions.

The elevation-dependent signature being less discernible in L2 than in L1 for some sites would be consistent with sea-surface effects being, in general, more significant for the shorter L1 wavelength (19 cm) than for the L2 wavelength (24 cm); this speculative hypothesis could not be validated with the available observations in this study and further testing is required. We tentatively explored this, for BUR2 and SPBY stations, where simultaneous observations of wind speed and direction were recorded with the TG data. For these two stations, the mean wind speed was projected across and along the mean azimuth direction of each observed satellite arc; however, neither correlation with the GNSS-RT levelling residuals nor difference between the across/along wind was found, in agreement with recent studies (e.g., Löfgren et al. 2014; Löfgren and Haas 2014). This outcome indicates that comparisons with local wind observations alone are likely not enough to approximate the complex sea-surface processes driven by roughness, swell, wave age and sea-surface anisotropies and asymmetries (Cardellach and Rius 2008; Cardellach et al. 2011).

The geometric multipath model of Eq. 1 does not consider the tropospheric refraction either which has three different effects on the observed phase delay. First, due to the reflector height, different tropospheric delay may affect the direct and reflected signals at low elevation as they traverse the troposphere along different paths. However, the refractivity for radio waves between 0 and 20 m height (the maximum reflector height among the case study sites, see Table 1) is less than 2 ppm (ITU 2012), which predicts a change in phase delay smaller than 1 mm at 5° elevation, and is thus negligible.

Second, the reflected signal traverses additional troposphere following the geometric excess path of Eq. 1. The excess path is proportional to the satellite elevation and reflector height; for a reflector height of 20 m, the excess path is 3.5 m at 5° elevation and increases to 20 m at 30° elevation. Using a standard radio refractivity for radio waves (315 ppm; ITU 2012), the predicted phase delay is ∼1 mm at 5° elevation and ∼6 mm at 30° elevation, respectively. Therefore, this effect may contribute to some extent to the differences observed in Table 2 above 12° elevation (values in parenthesis), but cannot explain the observed elevation-dependent bias.

Third, the bending of both the direct and reflected signals affects the elevation angle used in Eq. (1). Assuming a troposphere in hydrostatic equilibrium, the bending of the signals would produce a higher elevation angle which translates to a larger geometric delay in Eq. 1. The amplitude of the bending effect is similar for both GPS carriers reaching a maximum at low elevation angles and reducing exponentially as the satellite rises. Using the change in elevation angle reported by Roussel et al. (2014), the predicted phase delay change at 5° elevation is ∼14 cm for a reflector height of 20 m. At 30° elevation, the predicted delay is ∼1 cm. The elevation-dependent bending effect produces apparent lower reflector heights in agreement with the negative levelling bias found in L1 results below 12° elevation. We note,, however, that there is less elevation dependency observed in L2 than in L1 (Fig. 7), where the bending effect is the same. Also, the additional phase delay induced by bending is proportional to the reflector height, contradicting the elevation-dependent bias we found at different heights among the case study sites (from 3 to 20 m). Therefore, tropospheric refraction alone cannot explain the elevation-dependent bias observed.

Besides surface roughness and tropospheric refraction, an additional non-geometric contribution to the measured SNR that is unaccounted for in Eq. (1) results from the surface/antenna coupled response. We assumed an innocuous surface material with no elevation-dependent signature, as in a perfect electric conductor. Considering a surface material change between a perfect electric conductor and seawater within the SNR simulator developed by Nievinski and Larson (2014d), differences up to 6 cm were found in SNR-

estimated heights using real satellite arcs. The amplitude of the surface/antenna effect on the estimated SNR-heights may change with different antenna models and tracked signals. However, the simulated seawater surface provides systematically larger reflector heights (positive bias) with respect to the perfect electric conductor, which disagrees with the elevation-dependent bias found in Fig. 7. On the other hand, it would partially explain the height biases found at BUR2 and SPBY, which are equipped with the same antenna model and radome. Additionally, changes in the media permittivity are expected in time and between the case study sites due to different water temperature (average annual between 15 and 19 C) and salinity (average annual between 35 and 37.5 $^0/_{00}$). Considering water salinity variations only, differences smaller than 1 cm were found in simulated SNR observations where the reflecting surface was changed from seawater to fresh water. Actual salinity changes in seawater amongst the case study sites are one order of magnitude smaller than those simulated; therefore, they can be neglected. Although permittivity variations due to water temperature changes may still contribute to the differences in Table 2, they are undoubtedly not enough to explain the biases found for BUR2 and SPBY sites. Further research is needed to assess the impact of the antenna/surface contribution to the recorded SNR data.

The geometric model is also unable to differentiate between the contributions from additional reflectors or reflectors not being lower or horizontal with respect to the GNSS antenna. For instance, in SMTG there is a small cluster of reflecting points lying onshore from satellite arcs located between 90°–100° in azimuth (Fig. S1f). The GNSS-RT levelling estimates for these ground-reflected points are not distinguishable from those on the sea surface (see Fig. S1f), and furthermore, they are distributed randomly through the year and along the full sea-surface height from 2 to 12 m. Although these reflecting points seem to be located on the ground, it is very unlikely that they are produced by SNR oscillations from such a static reflector. A more reasonable, though speculative, explanation for these reflecting points is that they are produced by the Saint-Malo ferry which is occasionally located in the opposite direction to the reflecting points (see Fig. S2). When docked, the ferry represents a large reflecting object behind the antenna for those satellites between 90° and 100° in azimuth which moves consistently with the sea-surface height. This cluster of erroneous reflecting points can be easily detected and removed by visual inspection of the results (Fig. S1f); however, such manual intervention is limited by the available information of the station environment and is not consistent with the desired automatic methodology. For instance, we note that in Roscoff (ROTG) the available satellite images did not show recent port development near the station. Furthermore, visual inspection of the results does not identify reflections that originate from a different reflect-

ing object when the corresponding reflecting points are still being located on the sea surface.

This limitation is also noticed in Marseille (MARS), where a small number of reflecting points were obtained from terrestrial surfaces (Fig. S2). Due to the extremely low tidal range at this site (less than 0.4 m), SNR data from vertical or static reflecting objects were selected as they provided an oscillation indistinguishable from reflections off the sea surface. These invalid reflections are, however, sporadic and have no impact on the mean levelling value in MARS. Improving the SNR modelling of Eq. (1) may allow narrowing the bounds of the frequency estimate corresponding exclusively to sea-surface reflections. Alternatively, at sites such as MARS with a clear sea/ground separation, most of the ground surface can be masked with a simple azimuth range selection.

On the other hand, because of the surroundings of the GNSS antenna, reflections from the sea surface in SMTG are limited to very few and low satellite arcs; only 6 % of valid satellite arcs were retained at this site, from which 95 % are lower than 13°. For low-elevation reflections, the size of the reflecting footprint increases allowing for multiple non-water reflections to be integrated with the sea-surface reflection. This is critical in enclosed ports with multiple reflecting objects near the antenna such as at SMTG. These sparse and low elevation SNR observations, likely contaminated by the elevation-dependency of the GNSS-RT levelling results as well as tracking losses (more often in the weaker L2 carrier) and reflections from objects not conforming to the geometrical model, may explain why the L2 results from SMTG are significantly worse than for any other study site. We note that the recorded SNR resolution at SMTG and ROTG is 1 dB while for the other sites is between 0.05 and 0.25 dB depending on the receiver model. Low SNR resolution may impact the quality of the SNR oscillation at these two sites; for instance, it is unknown how the receiver rounds the SNR data into integer values (K. M. Larson, personal communication, 2014). Moreover, it would explain why the scatter of the levelling results for these two sites do not correspond with their high tidal range and are larger than the other case study sites.

Systematic differences between results in L1 and L2 are observed in Fig. 7 (see also Table 2), indicating that at some sites the GNSS-RT levelling results strongly depend on the GPS carrier used. The absolute differences between the mean GNSS-RT levelling estimates in L1 and L2 above 12° elevation for BUR2, SPBY and SMTG (15.5, 19.4, and 18.2 cm, respectively) are substantially larger than other sites (between 3 and 10.6 cm, with a median value of 3.8 cm). Despite selecting the SNR data that better adjust the oscillation model simultaneously in L1 and L2 (see Fig. 3), differences between L1 and L2 GNSS-RT levelling results may arise from receiver-dependent tracking issues leading to biases in the SNR measurement. Bilich et al. (2007) found

inconsistent SNR measurements among different manufacturers including correlation between L1 and L2 signals and spurious oscillations not related to the multipath environment.

SNR measurements in L2 using the P(Y) code are weaker than those in L1, and the resulting SNR frequency estimates are more sensitive to noise. SNR measurements with increased quality can be obtained from the L2C code transmitted by the GPS IIR-M satellites launched since 2005 (Larson et al. 2010). However, none of the sites studied here recorded L2C data despite many of them being capable of tracking it. The recording of L2C data depends on the receiver manufacturer, the signal tracking configuration set by the user and the data translation into a receiver-independent exchange format and its version. For instance, only one L2 phase and SNR observable are permitted to be recorded in the RINEX version 2.11 used here, with the L2P(Y) observable being preferred over the L2C for positioning/geodetic purposes. The GNSS-RT levelling approach would benefit from the newer and more flexible RINEX version 3 to use SNR phase observations from L2C. Alternatively, the raw binary file or an additional RINEX file containing L2C for reflectometry could be archived at each site.

A further examination of levelling errors related to the GNSS-RT technique errors was carried out to assess possible scale errors in the estimated heights. The antenna height above the sea surface varies more than 7 m at BRST, ROTG and SMTG sites. Figure 8 shows the non-overlapping running median estimated with 0.5 m SSH windows for both L1 (left) and L2 (right) at these three sites. Although the curves for ROTG and SMTG are noisier than for BRST, especially in L2, a common trend is seen in these three sites, where differences with respect to the nominal levelling values increase at lower SSH, i.e., the error in the SNR-estimated height is proportional to the vertical distance to the reflecting surface. The estimated linear trends of the GNSS-RT levelling results against SSH, or scale errors, for these three sites are between 0.6 and 1.4 cm/m, with a formal 1-sigma uncertainty smaller than 0.2 cm/m. Similar values for the trend are found in BRST and ROTG stations if one considers the GNSS-RT levelling results with satellite elevation above 12° only, i.e., it is not significantly correlated with the satellite elevation angle. It is feasible that such a scale error could originate from a tidal range error within the TG observations (see Sect. 5.2), though the amplitude is much larger than the error found in TGs with known tidal range errors (Martin Miguez et al. 2008b). Using data from three permanent GNSS sites, Nievinski and Larson (2014c) found that GNSS reflections underestimate snow depth estimates, i.e., the estimated antenna height above the reflecting surface is larger with a higher (closer) reflecting surface, consistent with our results. Nevertheless, the scale error reported in the latter study was one order of magnitude larger (between 5
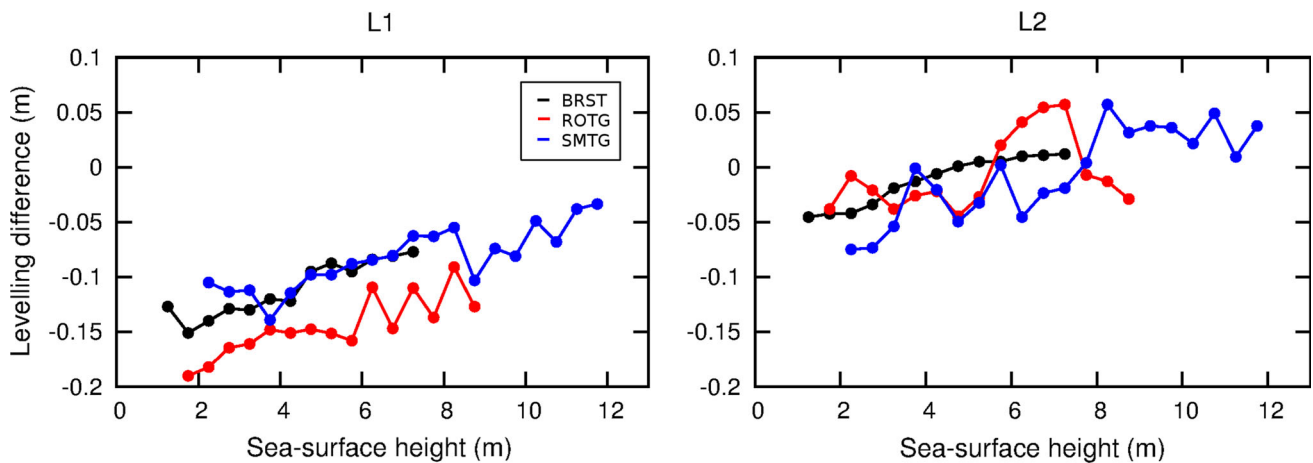
Fig. 8 Non-overlapping running median of the GNSS-RT levelling differences with respect to sea-surface height at BRST (*black lines*), ROTG (*red lines*) and SMTG (*blue lines*) for both L1 (*left*) and L2 (*right*) GPS signals. An offset of −0.3 m was removed from the SMTG L2 running median for visibility reasons

and 15 %), which may be related to their in situ data not being truly representative of the local environment or due to the spatial variation of snow density and subsequent signal penetration, which are both absent from the water surface case.

5.2 Errors in the TG, phase centre and in situ levelling data

The SSH observed by the TGs is directly added to the GNSS-RT height estimate to compute the levelling; any error in the SSH derived from the TG observations would thus map entirely into an error of the GNSS-RT levelling estimate. For instance, the instantaneous TG measurements of the water level inside a stilling well may not be representative of the external water level actually sensed by the GNSS antenna, due to for instance, the presence of significant swell, a different water density inside the well and/or the behaviour of the well orifices in the presence of waves or currents (Pugh 1996). Errors in the TG observations may also include instrumental noise, scale biases and clock shifts (Martin Miguez et al. 2008b).

The scale bias arises when the TG is not correctly measuring the actual tidal range from peak to peak, but a different (scaled) quantity. Noise at the level of 1–2 cm has been reported in TG observations for Brest, Roscoff and Saint-Malo (Martin Miguez et al. 2008a); however, it has little impact on the mean GNSS-RT levelling differences as changing the TG sampling between 6 or 10 min and 1 h, with different noise content, produces similar results at all sites. Also at Brest, observations from an acoustic TG co-located in the same stilling well provided similar results as the preferred radar TG. Larger effects such as TG observations mistakenly being truncated at the decimetre level were found and corrected for the Socoa station.

TG observations are also affected by datum errors that would appear as GNSS-RT levelling biases. Using our methodology, we identified a vertical offset of 1.5 cm in the BRST levelling time series around April 2013 (Fig. 5). No hardware/firmware change has been reported at the GNSS station at this epoch; however, the epoch of the offset exactly matches with a gap in the TG data when the radar sensor was replaced. Despite the location of the TGZ being re-established at the same reference after the sensor change, the vertical offset indicates a different TG reference before and after the sensor change. This outcome indicates that the GNSS-RT levelling could also be used to monitor the relative stability of both the GNSS and TG references.

As for the classical levelling campaigns, in situ validation of the TG performance is a demanding and costly operation; it requires a simultaneous reference gauge that is more accurate than the TG being controlled. The GNSS-RT levelling approach could provide the TG community with an independent assessment of discontinuities of sea-level data on a remote and continuous basis, provided the TG is co-located with an appropriate GNSS installation. Such a GNSS at TG configuration is recommended by GLOSS (IOC 2012) for the purposes of measuring vertical movement of the TG itself. For the BUR2 and SPBY sites, although they are equipped with the same TG model and installation, an error in the TG reference that could explain the GNSS-RT levelling biases has not been identified (Bureau of Meteorology, personal communication, 2014).

Errors in the vertical component of the calibrated antenna phase centre for any of the GNSS signals would map into a carrier-dependent levelling bias when compared to classical levelling, where only the height to the ARP is considered. In this regard, differences in the vertical component of the GNSS antenna phase centre between individual calibrations

have been reported close to 1 cm (Baire 2013), which may contribute to the mean levelling differences of Table 2. Note that the GNSS-RT technique is not affected by errors in the calibrated antenna phase centre values. Stations BUR2 and SPBY are the only ones equipped with a radome, but the large bias shown by these two stations in L1 cannot be explained by the effect of the radome which was also included in the antenna calibration model (Schmid et al. 2007).

Finally, through analysis of the case study sites presented here, several errors were found in the classical levelling values used as ground truth. Transcription and reduction mistakes in the reported nominal levelling values were found and corrected for MARS, SMTG and TARI sites. However, no error in the levelling data was found for the BUR2 and SPBY sites.

6 Conclusions

We have developed an approach based on the GNSS-R technique to obtain the ellipsoidal height of the TG reference point. The approach, termed GNSS reflectometry tie (GNSS-RT), estimates in a remote and continuous way the levelling connection between the reference points of co-located GNSS and TG stations. We analysed the frequency of SNR oscillations in the tracked GPS signals to derive the GNSS antenna height above the reflecting sea surface; this analysis utilised simultaneous SSH observations from the TG which ultimately yielded the levelling estimate.

We have shown how the detection of reflections from the sea surface can be improved using the a priori information of the time-variable SSH provided by the TG, even at sites with spatially complex and obstructed sea-surface reflections. We used the observed SSH variations to remove the non-linear changes in the frequency of the SNR oscillations, following an inverse Doppler-like effect, due to changes of the vertical distance to the sea surface. Furthermore, we were able to optimise the frequency estimate of the SNR oscillations by considering the SNR data dominated by reflections from the sea surface. Previous studies depended on manually establishing a station-specific azimuth and elevation mask. In contrast to those studies, we were able to isolate the reflected signals off the sea surface with no a priori knowledge of the relative location of the GNSS antenna and the objects blocking the reflections from the sea surface. This is an important advantage if this approach is to be used for operational levelling between the GNSS and TG reference marks.

We assessed the GNSS-RT levelling approach against in situ levelling campaigns at eight case study sites, each with a different daily tidal range and height above the sea surface. Using satellite observations above 12° elevation, the comparison at the case study sites yielded mean absolute differences at the centimetre level for L1 (absolute median value of 1.4 cm) and L2 (absolute median value of 2.3 cm), with four sites showing differences of 3 cm or smaller. We also exposed a number of current limitations of the simple multipath geometric model we adopted:

1. A clear elevation-dependent error below 12° elevation was observed in the GNSS-RT derived levelling, probably originating from tropospheric refraction and/or sea-surface roughness. This error was most obvious in the results from the L1 GPS signal.
2. At the Burnie (BUR2) and Spring Bay (SPBY) sites, large differences of more than 15 cm were detected between GNSS-RT levelling estimates using L1 and L2 GPS signals, including a bias of ∼10 cm in L1 that remains unexplained. Differences between L1 and L2 results are attributed to receiver-dependent approaches of measuring the SNR and require further detailed investigation.
3. A scale error (i.e., estimated heights proportional to the distance to the reflecting surface) of 0.6–1.4 cm/m was detected, being most apparent at sites with large SSH variation; and
4. reflections from objects not conforming to the geometric model still can provide levelling estimates indistinguishable from true reflections from the sea surface. This is especially the case when the object is floating (and thus subject to the same tidal variation) or in such cases where the tidal variation is very small (and thus our strategy is less effective at automatically isolating the sea level reflections).

The mean levelling differences we found may reflect errors in the TG reference and/or in the nominal levelling values used as ground truth, which includes in situ levelling errors and antenna PCO errors. Therefore, the reported levelling differences represent an upper error bound of the GNSS-RT technique. For instance, we identified a vertical offset of 1.5 cm at Brest coincident with a change in the TG sensor; highlighting that this approach potentially provides the TG community with a promising technique to remotely and automatically monitor the stability of the TG measurements.

Results with GPS data sampling at 30 s were similar to those with data sampling at 1 s, though the latter have a smaller scatter per satellite arc. A slower sampling rate of the SNR observations imposes a limit on the observable height of the GNSS antenna above the reflecting surface. We obtained an empirical upper limit of 16 m for 30 s SNR data, which is suitable for most coastal GNSS installations opening the application of the GNSS-RT levelling to larger sets of GPS stations co-located with TGs.

Further research is needed to reduce the errors in the GNSS-RT derived levelling estimates. In particular, further understanding of the non-geometric effects contained in the interferometric phase measured by the GNSS receivers such

as the sea surface roughness, tropospheric delay (including the bending effect) and the antenna/surface response. In addition, the positive results obtained with the L2P(Y) signal, where the elevation-dependency of the GNSS-RT estimates is less significant, encourage the use of the new transmitted L2C code which would provide increased quality of the SNR measurements for GNSS-RT levelling. Such perspective requires, however, the production of parallel RINEX files containing this SNR observable, which otherwise is not commonly included in GPS data repositories.

References

Amos MJ, Featherstone WE (2009) Unification of New Zealand's local vertical datums: iterative gravimetric quasigeoid computations. J Geod 83:57–68. doi:10.1007/s00190-008-0232-y

Andersen OB, Knudsen P (2009) DNSC08 mean sea surface and mean dynamic topography models. J Geophys Res 114:1–12. doi:10.1029/2008JC005179

Anderson KD (2000) Determination of Water Level and Tides Using Interferometric Observations of GPS Signals. J Atmos Oceanic Technol 17:1118–1127. doi:10.1175/1520-0426(2000)017<1118:DOWLAT>2.0.CO;2

Axelrad P, Larson K, Jones B (2005) Use of the correct satellite repeat period to characterize and reduce site-specific multipath errors. In: Proceedings of the 18th international technical meeting of the Satellite Division of The Institute of Navigation, ION GNSS 2005. pp 2638–2648

Baire Q et al (2013) Influence of different GPS receiver antenna calibration models on geodetic positioning. GPS Solut 18:1–11. doi:10.1007/s10291-013-0349-1

Benton CJ, Mitchell CN (2011) Isolating the multipath component in GNSS signal-to-noise data and locating reflecting objects. Radio Sci 46:RS6002. doi:10.1029/2011RS004767

Bilich A, Axelrad P, Larson KM (2007) Scientifc utility of the signal-to-noise ratio (SNR) reported by geodetic GPS receivers. Paper presented at the Proceedings of the 20th international technical meeting of the Satellite Division of The Institute of Navigation (ION GNSS 2007), Fort Worth, 25–28 Sept 2007

Bilich A, Larson KM (2007) Mapping the GPS multipath environment using the signal-to-noise ratio (SNR). Radio Sci 42:RS6003. doi:10.1029/2007rs003652

Bourlier C, Pinel N, Fabbro V (2006) Illuminated height PDF of a random rough surface and its impact on the forward propagation above oceans at grazing angles. In: Antennas and propagation, 2006. EuCAP 2006. First European conference on, 6–10 Nov 2006, pp 1–6. doi:10.1109/EUCAP.2006.4584894

Calafat FM, Chambers DP, Tsimplis MN (2014) On the ability of global sea level reconstructions to determine trends and variability. J Geophys Res 119:1572–1592. doi:10.1002/2013JC009298

Cardellach E, Rius A (2008) A new technique to sense non-Gaussian features of the sea surface from L-band bi-static GNSS reflections. Remote Sens Environ 112:2927–2937. doi:10.1016/j.rse.2008.02.003

Cardellach E, Fabra F, Nogués-Correig O, Oliveras S, Ribó S, Rius A (2011) GNSS-R ground-based and airborne campaigns for ocean, land, ice, and snow techniques: application to the GOLD-RTR data sets. Radio Sci 46:RS0C04. doi:10.1029/2011RS004683

Church J, White N (2011) Sea-level tise from the Late 19th to the Early 21st Century. Surv Geophys 32:585–602. doi:10.1007/s10712-011-9119-1

Dayoub N, Moore P, Penna NT, Edwards SJ (2012) Evaluation of EGM2008 within geopotential space from GPS, tide gauges and altimetry. In: Kenyon S, Pacino MC, Marti U (eds) Geodesy for planet earth. International Association of Geodesy Symposia, vol 136. Springer, Berlin, Heidelberg, pp 323–331. doi:10.1007/978-3-642-20338-1_39

Elosegui P, Davis JL, Jaldehag RTK, Johansson JM, Niell AE, Shapiro II (1995) Geodesy using the global positioning system: the effects of signal scattering on estimates of site position. J Geophys Res 100:9921–9934

Featherstone WE, Filmer MS (2012) The north-south tilt in the Australian height datum is explained by the ocean's mean dynamic topography. J Geophys Res 117:C08035. doi:10.1029/2012JC007974

Foreman MGG, Crawford WR, Cherniawsky JY, Galbraith J (2008) Dynamic ocean topography for the northeast Pacific and its continental margins. Geophys Res Lett 35:L22606. doi:10.1029/2008GL035152

Georgiadou Y, Kleusberg A (1988) On carrier signal multipath effects in relative GPS positioning. Map Collect 13:172–179

Holgate SJ et al (2013) New data systems and products at the permanent service for mean sea level. J Coast Res 29:493–504. doi:10.2112/jcoastres-d-12-00175.1

IOC (2006) Manual on sea-level measurement and interpretation: an update to 2006. IOC manuals and guides no. 14, vol IV, JCOMM technical report no. 31, WMO/TD. No. 1339. Intergovernmental Oceanographic Commission of UNESCO, Paris, p 78 (English)

IOC (2012) Global sea-level observing system (GLOSS) implementation plan—2012. IOC technical series no. 100. UNESCO/IOC, p 41 (English)

ITU (2012) The radio refractive index: its formula and refractivity data. ITU-R recommendation P.453-12, P-series, p 30

Jacobson MD (2010) Snow-covered lake ice in GPS multipath reception—theory and measurement. Adv Space Res 46:221–227. doi:10.1016/j.asr.2009.10.013

Jin S, Cardellach E, Xie F (2014) GNSS remote sensing: theory, methods and applications. Remote sensing and digital image processing, vol 19. Springer, Netherlands. doi:10.1007/978-94-007-7482-7

Koohzare A, Vaníček P, Santos M (2008) Pattern of recent vertical crustal movements in Canada. J Geodyn 45:133–145. doi:10.1016/j.jog.2007.08.001

Larson K, Nievinski F (2013) GPS snow sensing: results from the EarthScope Plate Boundary Observatory. GPS Solut 17:41–52. doi:10.1007/s10291-012-0259-7

Larson KM, Small EE, Gutmann ED, Bilich AL, Braun JJ, Zavorotny VU (2008) Use of GPS receivers as a soil moisture network for water cycle studies. Geophys Res Lett 35:L24405. doi:10.1029/2008gl036013

Larson KM, Gutmann ED, Zavorotny VU, Braun JJ, Williams MW, Nievinski FG (2009) Can we measure snow depth with GPS receivers? Geophys Res Lett 36:L17502. doi:10.1029/2009gl039430

Larson KM, Braun JJ, Small EE, Zavorotny VU, Gutmann ED, Bilich AL (2010) GPS multipath and its relation to near-surface soil moisture content. selected topics in applied earth observations and remote sensing. IEEE J 3:91–99. doi:10.1109/jstars.2009.2033612

Larson KM, Löfgren JS, Haas R (2013a) Coastal sea level measurements using a single geodetic GPS receiver. Adv Space Res 51:1301–1310. doi:10.1016/j.asr.2012.04.017

Larson KM, Ray RD, Nievinski FG, Freymueller JT (2013b) The accidental tide gauge: a GPS reflection case study From Kachemak Bay, Alaska. IEEE Geosci Remote Sens Lett 10:1200–1204. doi:10.1109/lgrs.2012.2236075

Löfgren JS, Haas R, Johansson JM (2011a) Monitoring coastal sea level using reflected GNSS signals. Adv Space Res 47:213–220. doi:10.1016/j.asr.2010.08.015

Löfgren JS, Haas R, Scherneck HG, Bos MS (2011b) Three months of local sea level derived from reflected GNSS signals. Radio Sci 46:RS0C05. doi:10.1029/2011RS004693

Löfgren JS, Haas R (2014) Sea level measurements using multi-frequency GPS and GLONASS observations. EURASIP J Adv Signal Process 2014:50. doi:10.1186/1687-6180-2014-50

Löfgren JS, Haas R, Scherneck HG (2014) Sea level time series and ocean tide analysis from multipath signals at five GPS sites in different parts of the world. J Geodyn. doi:10.1016/j.jog.2014.02.012

Madsen KS, Høyer JL, Tscherning CC (2007) Near-coastal satellite altimetry: sea surface height variability in the North Sea-Baltic Sea area. Geophys Res Lett 34:L14601. doi:10.1029/2007GL029965

Martin Miguez B, Le Roy R, Woeppelmann G (2008a) The use of radar tide gauges to measure variations in sea level along the French coast. J Coast Res 24:61–68. doi:10.2112/06-0787.1

Martin Miguez B, Testut L, Woppelmann G (2008b) The Van de Casteele test revisited: an efficient approach to tide gauge error characterization. J Atmos Oceanic Technol 25:1238–1244. doi:10.1175/2007jtecho554.1

Nievinski F, Larson K (2014a) Forward modeling of GPS multipath for near-surface reflectometry and positioning applications. GPS Solut 18:309–322. doi:10.1007/s10291-013-0331-y

Nievinski FG, Larson KM (2014b) Inverse modeling of GPS multipath for snow depth estimation—part I: formulation and simulations. IEEE Trans Geosci Remote Sens 52:6555–6563. doi:10.1109/TGRS.2013.2297681

Nievinski FG, Larson KM (2014c) Inverse modeling of GPS multipath for snow depth estimation—part II: application and validation. IEEE Trans Geosci Remote Sens 52:6564–6573. doi:10.1109/TGRS.2013.2297688

Nievinski FG, Larson KM (2014d) An open source GPS multipath simulator in Matlab/Octave. GPS Solut 18:1–9. doi:10.1007/s10291-014-0370-z

Penna NT, Featherstone WE, Gazeaux J, Bingham RJ (2013) The apparent British sea slope is caused by systematic errors in the levelling-based vertical datum. Geophys J Int 194:772–786. doi:10.1093/gji/ggt161

Press WH, Teukolsky SA, Vetterling WT, Flannery BP (2001) Numerical recipes in Fortran 77: the art of scientific computing, vol 1, 2nd edn. Cambridge University Press, New York

Pugh DT (1996) Tides, surges and mean sea-level (reprinted with corrections). Wiley, Chichester

Roussel N, Frappart F, Ramillien G, Desjardins C, Gegout P, Pérosanz F, Biancale R (2014) Simulations of direct and reflected waves trajectories for in situ GNSS-R experiments. Geosci Model Dev Discuss 7:1001–1062. doi:10.5194/gmdd-7-1001-2014

Sánchez L (2012) Towards a vertical datum standardisation under the umbrella of global geodetic observing system. J Geod Sci 2:325–342. doi:10.2478/v10156-012-0002-x

Schmid R, Steigenberger P, Gendt G, Ge M, Rothacher M (2007) Generation of a consistent absolute phase-center correction model for GPS receiver and satellite antennas. J Geod 81:781–798. doi:10.1007/s00190-007-0148-y

Small EE, Larson KM, Braun JJ (2010) Sensing vegetation growth with reflected GPS signals. Geophys Res Lett 37:L12401. doi:10.1029/2010gl042951

Watson C, White N, Church J, Burgette R, Tregoning P, Coleman R (2011) Absolute calibration in Bass Strait, Australia: TOPEX, Jason-1 and OSTM/Jason-2. Mar Geod 34:242–260. doi:10.1080/01490419.2011.584834

Woodworth PL, Hughes CW, Bingham RJ, Gruber T (2012) Towards worldwide height system unification using ocean information. J Geod Sci 2:302–318. doi:10.2478/v10156-012-0004-8